RESEARCH ARTICLE

Combination of a chemopreventive agent and paclitaxel in CD44-targeted hybrid nanoparticles for breast cancer treatment

Bao Ngoc Tran[1] · Hanh Thuy Nguyen[2,3] · Jong Oh Kim[2] · Chul Soon Yong[2] · Chien Ngoc Nguyen[1,3]

Abstract The CD44 receptor, which is upregulated in many cancer cells, provides a selective cellular surface for targeted drug delivery systems. We developed a hybrid nanocarrier for the CD44-targeted delivery of ibuprofen (IBU) and paclitaxel (PTX). The solid lipid nanoparticles (SLNs) were prepared by a hot-melt oil/water emulsion technique and then coated with hyaluronic acid (HA) by electrostatic interactions. The final SLN were spherical with a hydrodynamic diameter (Z) of 72.16 ± 2.9 nm, polydispersity index (PDI) of 0.276 ± 0.009, and zeta potential (ZP) of 28.20 ± 0.69 mV. Similarly, SLN coated with HA (SLN-HA) exhibited acceptable physical properties (Z 169.3 ± 0.55 nm, PDI 0.285 ± 0.004, and ZP $- 10.5 \pm 0.15$ mV). Cell viability assays showed that the combination of IBU, a chemopreventive agent, and PTX exerted a synergistic inhibitory effect on the proliferation of cancer cells (CI < 1.0). Additionally, our observations indicated that both SLN and SLN-HA enhanced apoptosis and cellular uptake compared to the cocktail of free drugs. HA indicated its affinity for cancer cells through the improvement of cellular uptake and induction of apoptosis.

These results clearly indicated that these nanoparticle systems hold great promise for drug delivery in breast cancer treatment.

Introduction

Recent reports suggest that commonly used non-steroidal, anti-inflammatory drugs (NSAIDs), such as aspirin and ibuprofen (IBU), which exert their clinical activity through the COX inhibition, can inhibit the proliferation and induce cytotoxicity of many types of cancer cells. This was attributable to the greater expression of COX-2 in human cancer cells than in non-cancerous cells (Taketo 1998a, b) and that the upregulation of COX-2 promotes tumor-specific angiogenesis, inhibits apoptosis, and induces pro-angiogenic factors (Yao et al. 2005). IBU improved the sensitivity of cancer cells when co-administered with popular chemotherapeutic agents (Wood et al. 2011; Endo et al. 2014; Ouakrim et al. 2015; Thakkar et al. 2015) and significantly reduced the incidence, multiplicity, and volume of breast tumors (40, 52, and 57%, respectively; p < 0.001) (Harris et al. 2000). NSAIDs are less toxic than common anti-cancer agents; however, the required dose for anti-tumor effects is much higher than that for COX inhibition (Smalley and DuBois 1997). Nevertheless, it is reasonable to consider the combination of IBU, a chemopreventive agent, with a conventional chemotherapeutic agent would produce synergistic clinical effects on cancer cells (Endo et al. 2014). In this study, paclitaxel (PTX) was combined with IBU and the effects on breast cancer cell-lines were evaluated.

Bao Ngoc Tran and Hanh Thuy Nguyen have equally contributed.

✉ Chul Soon Yong
csyong@yu.ac.kr

✉ Chien Ngoc Nguyen
nguyenngocchien@yahoo.com; chiennn@hup.edu.vn

[1] Department of Pharmaceutical Industry, Hanoi University of Pharmacy, Hanoi, Vietnam

[2] College of Pharmacy, Yeungnam University, Gyeongsan, South Korea

[3] National Institute of Pharmaceutical Technology, Hanoi University of Pharmacy, Hanoi, Vietnam

PTX has been indicated for the treatment of a variety of solid tumors. New nanoscale formulations, such as solid lipid nanoparticles (SLNs) and liposomes, are promising PTX delivery systems. Nanoparticles overcome the poor solubility of PTX and resolve several problems of systemic administration (Fonseca et al. 2002; Danhier et al. 2009). The PTX–IBU combination is an effective strategy to increase anticancer activity, reduce toxicity, and prevent drug resistance; lipid nanoparticles with a solid matrix, also called SLNs, may be useful for the delivery of this combination. SLNs have several advantages over conventional delivery systems, including enhancement of the ability of the drug to cross the cellular barriers and an increased drug stability and solubility. The most important advantage is the increased bioavailability of lipophilic drugs (Potta et al. 2011; Tran et al. 2014; Thakkar et al. 2015).

As cytotoxic treatment drugs should be targeted specifically to the cancer cells, targeting agents that bind cell surface receptors are a useful approach. Hyaluronic acid (HA), a high-molecular weight linear glycosaminoglycan composed of repeated disaccharide units of β-1,4-D-glucuronic acid–β-1,3-N-acetyl-D-glucosamine, has a high binding capacity with several receptors, such as the CD-44, RHAMM, LYVE-1, IVd4, and LEC receptors (Sherman et al. 1994; Mero and Campisi 2014). The interaction of CD44 and HA has been commonly used in tumor targeting (Segura et al. 2005; Tran et al. 2014; Pradhan et al. 2015). CD44 receptors are structurally and functionally diverse, responsible for varied roles such as cell adhesion, cell orientation, migration, and chemoresistance (Murohashi et al. 2010), and CD44 promoted cancer stem cell "homing" in several solid tumors of breast cancers such as the MDA-MB-231, MDA-MB-436, and HBL-100 cell lines (Sheridan et al. 2006; Jin et al. 2016). The interaction of HA (also called hyaluronan) synthesized by cells with CD44 initiates signaling procedures related to ductal carcinoma or metastasized tumors. The binding of HA to an isoform of CD44 (CD44s) promoted breast cancer cell adhesion and inhibited invasion. In contrast, the binding of HA to CD44v3 led to tumor infiltration, cancer metastases, and clinical cases in which CD44v7-v8 expression was observed were reported to be associated with poorer disease outcomes and low survival rate (Watanabe et al. 2005; Toole 2009; Basakran 2015). The disruption of hyaluronan–CD44 signaling may improve the tumor response to conventional anticancer drugs. Therefore, a chemotherapeutic agent that cooperatively functions with HA is a promising approach for CD44-targeted therapies (Ponta et al. 2003; Götte and Yip 2006).

The conjugation of HA onto liposomes for the efficient diagnosis and treatment of cancer by targeted delivery or cell-labelling based on CD44 interactions has become popular (Esposito et al. 2008; Arpicco et al. 2013; Hayward et al. 2016; Ravar et al. 2016; Tran et al. 2017). However, the combination of two drugs with different physicochemical properties in the liposome would present disadvantages such as poor shelf-life and leakage of the contained drugs; consequently, the drug release may not occur as expected. Compared with liposomes, which have been used from 1965, SLNs, which were identified in 1991, have higher physical stability and can perform controlled drug delivery. Different drugs can be loaded into their lipid core with a high entrapment efficacy and concurrently delivered into cells (Mueller et al. 2000; Garud et al. 2012; Naseri et al. 2015).

In this study, we hypothesized that HA-coated SLN (SLN-HA), encapsulating a combination of PTX and IBU, could exert improved anti-cancer effects. The optimized formulations of SLN and SLN-HA were selected based on physicochemical properties [including particle size (Z), zeta potential (ZP), size distribution (polydispersity index, PDI), and particle morphology]. The optimized formulations were then evaluated for in vitro cytotoxicity efficacy, cellular uptake, and cell apoptosis in CD44⁻ (BT-474) and CD44⁺ breast cancer cell lines (MDA-MB-231).

Materials and methods

Material

IBU was purchased from the National Institute of Drug Quality Control (Hanoi, Vietnam). PTX was obtained from Sinopharm (Beijing, China). Polysorbate 80 (T80) was purchased from Duksan Chemical Co. (Ansan, South Korea). Stearyl cetyl alcohol (SCA) was purchased from the Thai Fatty Alcohols Co. (Bangkok, Thailand). Didodecyldimethylammonium bromide (DDAB), 3-(4,5-dimethyl-2-thiazolyl)-2,5-diphenyl tetrazolium bromide (MTT) reagent, and coumarin-6 were purchased from Sigma-Aldrich (St. Louis, MO, USA). HA (3 kDa) was supplied by B&K Technology Group Co. Ltd. (Xiamen, China). All other chemicals were of reagent grade and were used without further purification.

Preparation of combined IBU–PTX-loaded SLN

SLN was prepared by using the hot melt oil-in-water (o/w) emulsification technique as described in previous studies (Sutaria et al. 2012; Tran et al. 2014; Thakkar et al. 2015). The oil phase containing IBU, PTX, and DDAB was dissolved in hot-melt SCA at 80 °C. The aqueous phase was prepared by the dissolution of Tween 80 (T80) in 10 mL water. The compositions are presented in Table 1.

The melted lipid phase was homogenized into the hot aqueous phase (80 °C) by continuous sonication at 80 W

Table 1 Composition of SLN and SLN-HA

| Nos. | SLN nanosuspension | | | | | |
	Drugs[a] (mg)	SCA (mg)	DDAB (mg)	Water (mL)	Tween 80 (% in water)	HA (%)[b]
1	10	40	5	10	0	
2	10	40	5	10	0.5	
3	10	40	5	10	1	
4	10	40	5	10	3	
5	10	40	0	10	1	
6	10	40	10	10	1	0
7	10	40	20	10	1	
8	10	40	10	10	1	0.5
9	10	40	10	10	1	1
10	10	40	10	10	1	1.5

[a]Drugs (mg) refers to the total weight of IBU and PTX, the ratio of PTX:IBU was 1:4 (w/w)

[b]HA refers to the concentration of HA solution added to the SLN nanosuspension

by using a high intensity probe ultrasonic processor Vibra-Cell (Sonics and Materials, Newtown, CT, USA). Then, the obtained emulsion was cooled by magnetic stirring at 1200 rpm (Ika RCT basic IKAMAG, Staufen, Germany) for 15 min in an ice-cold water bath. The emulsifier and free drugs were washed away by ultra-filtration (MW 10,000, Millipore, Billerica, MA, USA) to obtain the final SLN. Drug-free SLN was produced in a similar fashion, but without the addition of drugs.

Preparation of HA-coated SLN (SLN-HA)

HA was coated onto the SLN surface via electrostatic interactions (Tran et al. 2014; Pradhan et al. 2015). One milliliter (mL) of HA aqueous solution (0–1.5% w/v) was added dropwise into SLN (10 mL) with mild stirring to obtain SLN-HA (Tran et al. 2017). The remained unbound HA was removed by ultra-filtration (MW 10,000, Millipore, Billerica, MA, USA) to obtain the final SLN. Drug-free SLN was used to produce drug-free SLN-HA.

Hydrodynamic diameter and zeta potential

The samples of SLN and SLN-HA were characterized through the measurement of their mean size (Z), PDI, and ZP by using a dynamic light scattering (DLS) system, Zetasizer Nano 90 (Malvern Instruments, Worcestershire, UK). For the Z and PDI analyses, the samples were loaded in polystyrene cuvettes; for ZP analysis, they were loaded in specifically designed "Folded Capillary Zeta Cell" cuvettes. Each measurement of samples diluted ten times with distilled water was conducted in triplicate. All the data were expressed as the mean ± standard deviation.

Morphological characterization of SLN and SLN-HA

The morphological studies of SLN and SLN-HA were conducted by using transmission electron microscopy (TEM). For TEM analysis, a small drop of SLN or SLN-HA was stained with 2% phosphotungstic acid solution, deposited onto a carbon-coated copper grid, and dried for 30 min at room temperature (25 °C). TEM images were recorded by using an H7600 transmission electron microscope (Hitachi, Tokyo, Japan).

Fourier transform infrared spectroscopy (FT-IR) analysis

The surface chemistry and physical interaction between polymers and drugs were determined from FT-IR spectra. The samples for FT-IR spectrometry were analyzed over the range from 650 to 4000 cm^{-1} by using a Thermo Scientific Nicolet Nexus 670 FT-IR Spectrometer and Smart iTR software (Thermo Fisher Scientific, Waltham, MA, USA).

Encapsulation efficiency

The encapsulation efficiency (EE) of SLN and SLN-HA for each drug (IBU and PTX) was determined after the centrifugation of 1 mL of the nanoparticle suspension in an ultrafiltration tube (MWCO, 10 kDa; Amicon Ultra, Millipore, MA, USA) and the assay of the free drug content of the filtrate. The EE values were calculated from the following equation:

$$EE\ (\%) = \left(W_{total\ drug} - W_{free\ drug}\right)/W_{total\ drug} \times 100,$$

where $W_{total\ drug}$ is the total amount of each drug in the final suspension and $W_{free\ drug}$ is the amount of drug in the filtrate. All the measurements were performed in triplicate.

The amounts of IBU and PTX were quantified simultaneously by high-performance liquid chromatography (HPLC). An Agilent 1260 Infinity LC system (Agilent Technologies, Palo Alto, CA, USA) and a Poroshell 120 SB-C18 column (15 cm × 0.30 cm, 2.7 μm) were employed. A mixture of 0.01 M phosphate buffer solution (pH 3.5) and acetonitrile (60:40, v/v) was used as the mobile phase, with a flow rate of 0.3 mL/min. The injection volume was 50 μL and the absorbance was detected at 220 nm. The calibration plots showed excellent linearity and the relative standard deviation of the plot over different time periods was below 3%.

In vitro drug release

The drug release study was conducted in pH 7.4 phosphate-buffered saline (PBS). Three milliliters of SLN or SLN-HA suspension was transferred into a dialysis bag (MWCO, 10 kDa; Membrane-Cel, Chicago, IL, USA). Each dialysis bag was kept inside a 50-mL tube containing 30 mL of release medium and incubated at 37 °C in a shaking water bath (Shaker Incubator LSI-100B, Beijing KWF Sci-tech Development, Beijing, China) with continuous shaking at 100 rpm. The release medium was prepared with 1% T80 because of the low solubility of PTX in water. At predetermined time points (after 1, 3, 5, 7, 9, 12, 24, 36, 48 h, respectively), 1 mL of the release medium was collected and replaced with an equal volume of fresh medium. The quantities of PTX and IBU released were assayed by using the HPLC method described above. The release experiments were performed in triplicate and the results were expressed as the mean ± SD.

Cell culture

Breast cancer cell-lines (BT-474 and MDA-MB-231) were originally obtained from the Korean Cell Bank (Seoul, South Korea). They were cultured in Dulbecco's modified Eagle's medium (HyClone Lab., South Logan, UT, USA) supplemented with 10% fetal bovine serum and 1% antibiotics at 37 °C. For cell treatment, all IBU and PTX solutions were prepared in the culture medium at indicated concentrations.

Cell viability assay

Cell viability analysis was performed by assaying mitochondrial dehydrogenase enzyme activity of the living cells via an MTT (3-(4, 5-dimethylthiazol-2-yl) 2, 5-diphenyltetrazolium bromide) assay. The cells (1×10^4 cells/well) were seeded in 96-well plates and incubated for 24 h. Thereafter, the cells were treated with blank SLN, free drugs, a combination of free drugs, SLN, and SLN-HA to compare the cell cytotoxicity of each sample within a selected range of concentrations (between 0.1 and 10 μg/mL). After incubation at 37 °C for 24 and 48 h, respectively, the cells were washed with PBS, treated with MTT solution (1.25 mg/mL in DMEM), and incubated again at 37 °C for 3 h, after which 100 μL DMSO was added to each well and the absorbance was measured at 570 nm by using a microplate reader. The relative viability of cells in samples treated with reagents versus control (untreated) samples was calculated from the following equation (Pradhan et al. 2015; Tran et al. 2015; Nguyen et al. 2017):

$$\text{Cell viability } (\%) = \left(\text{OD570}_{sample} - \text{OD570}_{blank}\right) / \left(\text{OD570}_{control} - \text{OD570}_{blank}\right) \times 100,$$

where OD represents the optical density measured at 570 nm.

The combination index (CI) was computed by CompuSyn 1.0 (CompuSyn, Paramus, NJ, USA), based on the method proposed by Chou and Talalay (Chou 2006). In this method, CI = 1 indicates an additive effect in the absence of synergism or antagonism, CI < 1 indicates synergism, and CI > 1 indicates antagonism (Chou and Talalay 1981, 1984).

Intracellular uptake analysis

The uptake of SLN into cells was evaluated by using confocal imaging and flow cytometric analysis (fluorescence-activated cell sorting, FACS; Nguyen et al. 2017; Thapa et al. 2017). BT-474 and MDA-MB-231 cells (1×10^5 cells/well) were separately seeded on coverslips placed in 12-well plates and incubated for 24 h. The cells were then treated with coumarin-6 loaded SLN and SLN-HA for 60 min at a coumarin-6 concentration of 0.5 μg/mL. In addition, the targeting ability of the SLN-HA formulation was determined by pretreatment with the free HA for 1 h at a concentration of 20 μg/mL. After the excess nanoparticles were removed by washing with PBS, the cells were fixed by the addition of 4% paraformaldehyde solution in the dark, the cover slips were then mounted and sealed on glass slides, and the samples were observed under a confocal laser scanning microscope (CLSM; K1-Fluo, Nanoscope Systems, Daejeon, Korea). The excitation wavelength was 494.0 nm and the emission wavelength was 518 nm for coumarin-6. Nikon-compatible filter cubes were green for viewing coumarin-6-labelled SLN uptake and blue for viewing stained nucleus, respectively.

The cancer cells were similarly cultured and treated in 12-well plates without coverslips. These cells were harvested by trypsin and then dispersed in 1.0 mL PBS for flow cytometric analysis by using a FACS Calibur flow cytometer (BD Biosciences, San Jose, CA, USA).

Apoptosis study

BT-474 and MDA-MB-231 cells (1×10^5 cells/well) were incubated for 24 h (37 °C) in 12-well plates. The cells were treated with free IBU, free PTX, mixture of free drugs, SLN, and SLN-HA at a drug concentration of 1 μg/mL for 24 h, and then washed with PBS. The mixture of free drugs, SLN, and SLN-HA were prepared with the PTX:IBU ratio determined by the previous cell viability assay. Hoechst staining (for nuclear apoptosis) was performed with 5 μg/mL Hoechst 33342 and the cells were incubated at room temperature (25 °C) for 15 min in the dark. The cells were then washed three times with PBS before being imaged by a fluorescence microscope (Nikon Eclipse Ti, Tokyo, Japan).

In addition, cellular apoptosis was evaluated by FACS analysis using an Annexin V kit assay (BD Biosciences, San Jose, CA, USA). Briefly, cells were collected and stained with Annexin-V and propidium iodide for 10 min in the dark and then the number of apoptotic cells were analyzed by using a FACS Calibur flow cytometer (BD Biosciences, San Jose, CA, USA) (Thapa et al. 2015).

Results

Preparation of SLN-HA

In order to obtain nanoscale particles (under 300 nm), SLNs were prepared with different concentrations of the surfactants, including T80 and DDAB, in the aqueous phase. The detailed compositions of the SLN formulations are shown in Table 1 and the details of their characterization based on ZP, Z, and PDI are shown in Fig. 1.

Effect of T80

The effects of T80 on Z, PDI, and ZP are illustrated in Fig. 1. All formulations with T80 had smaller Z values (under 200 nm) compared to the formulation without T80 (245 nm). The Z values were 72.1 ± 2.9, 27.2 ± 2.7, and 24.9 ± 1.1 nm at T80 concentrations of 0.5, 1, and 3%, respectively. In addition, the ZP values decreased from 61.9 to 17.9 mV as the T80 concentration increased from 0 to 3%. Based on these results, the SLN with the smallest particle size, of approximately 24 nm, was formed at a T80 concentration of 3%, but considered unstable because of

the small ZP (under 20 mV). The SLN formulation with 3% T80 recorded rather high PDI values (over 0.4) and a significant increase in Z was observed after storage for 24 h (data not shown). From the obtained results, the T80 concentration of 1% was chosen as the optimum as it yielded SLN with the most desirable characteristics: small Z (50 nm), low PDI (0.263), and high ZP values (27.2 mV).

Effect of DDAB

The effects of DDAB concentrations on SLN properties, especially ZP, were evaluated and the results are presented in Fig. 1b. The formulation prepared without DDAB had small and slightly negative ZP (approximately − 4.75 mV), which was not suitable for HA coating. As the DDAB content increased from 5 to 20 mg (0.05–0.2% in water), the ZP progressively increased from 14.3 to 69.2 mV, respectively. This confirmed that DDAB was located on the surface of the SLN. Thus, the reversal of ZP from negative to positive values was caused by an increased number of the quaternary ammonium cations of DDAB on the SLN surface. In addition, an increase in DDAB concentration reduced Z values. When the DDAB content was relatively high (20 mg), the particle size of the SLN was well below 50 nm, but fairly unstable during storage. Consequently, a DDAB content of 10 mg (0.1%) was considered to produce optimized SLN: Z of 72.16 ± 2.9 nm, PDI of 0.276 ± 0.009, and ZP of 28.2 ± 0.69 mV.

Effects of HA

The concentration-dependent effects of the conjugated HA on Z, PDI, ZP, and EE are indicated in Fig. 1c, d. An inverse relationship appeared to exist between HA concentration and ZP of the SLN-HA; when the HA concentration was increased from 0 to 1.5%, the ZP values were in the range from + 28.2 mV (without HA) to − 10.5 mV at 1.5% w/v HA. The process of ZP reversal from positive to negative values indicated that the HA molecules attached to the SLN surface. In Fig. 1c, it is shown that the mean diameter of particles steadily increased as more HA was embedded onto the SLN surface. The recorded Z values (from < 100 to 185 nm) corresponded well with the rise of HA concentration (from 0 to 1.5%). The saturation of HA embedding onto the surface of SLN was reported when the HA content was increased from 1 to 1.5% (Z and ZP were not significantly different). Therefore, the optimal HA concentration selected was 1%. The final SLN-HA properties were: Z 169.3 ± 0.55 nm, PDI 0.285 ± 0.004, and ZP − 10.56 ± 0.15 mV.
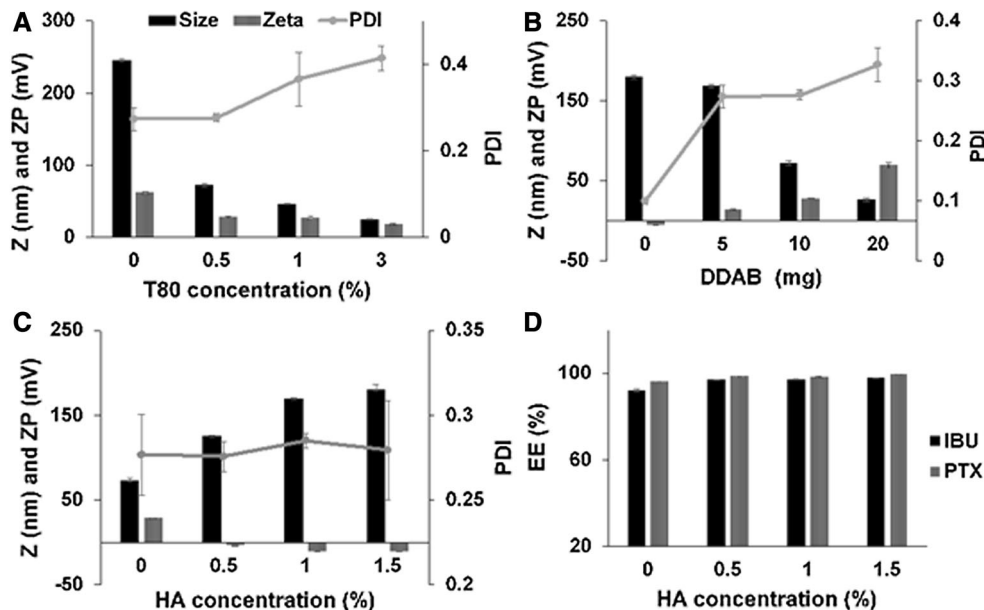
Encapsulation efficiency

The EE values were calculated for SLN alone as well as for SLN-HA with different HA concentrations; the results are presented in Fig. 1d. In general, EE values were over 90%. In the SLN system, the EE value of IBU (91.9%) was lower than that of PTX (96.1%), which can be explained by the higher solubility of IBU in water than PTX and because the smaller IBU molecules leak more easily from the SLN. However, in case of SLN-HA, both drugs had EE values with no significant difference (around 97%); this was attributed to the role of the thick layer of HA covering, which retains the drugs inside the nanostructures.

Morphological characterization

The morphology of SLN and SLN-HA is reported in Fig. 2. The TEM images shown in Fig. 2a, b confirmed the Z values recorded by DLS technology (Fig. 1c), which showed that the SLNs and SLN-HA had spherical morphology. The Z of SLN was approximately 70 nm (Fig. 2a), whereas the Z of SLN-HA was approximately 170 nm (Fig. 2b). This confirmed that the coating HA onto the SLN surface increased the diameter of the nanoparticle.

The FT-IR spectra of SLN-HA, SLN, and formulation components, including IBU, PTX, DDAB, and SCA, are shown in Fig. 2c. The red line represents the FT-IR spectrum of SLN and the black line represents the spectrum of SLN-HA. In general, the peak and pattern of the SLN spectrum were similar to those of the green spectrum (SCA), which indicated that SCA was an important platform for a reservoir for the drugs and surfactants. In addition, because SCA was used in the highest proportion
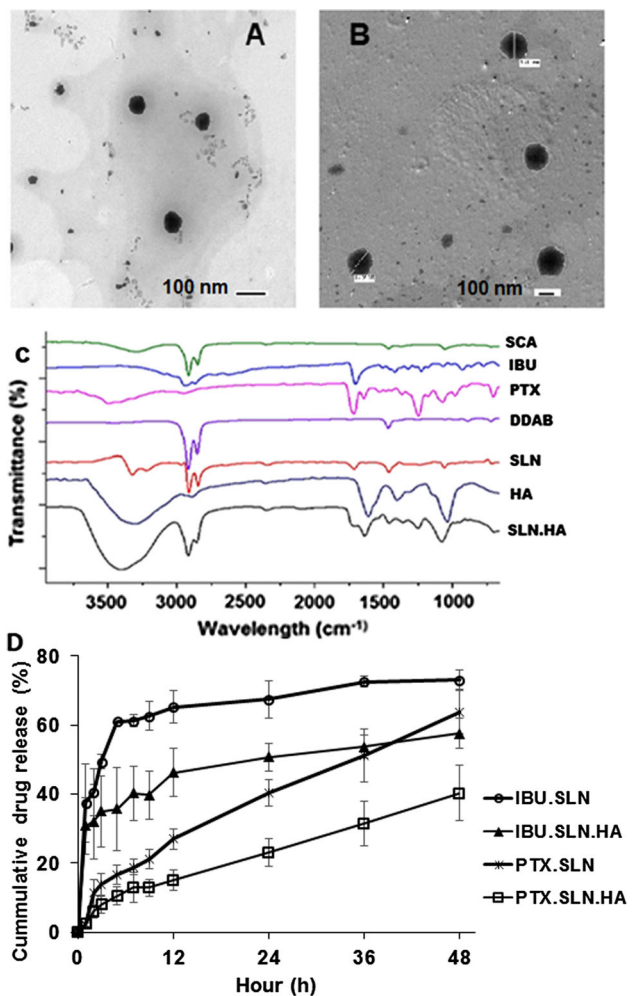

Fig. 2 Physicochemical properties of SLN and SLN-HA: TEM images of SLN (**a**) and SLN-HA (**b**), FT-IR (**c**), and in vitro drug release (**d**)

in the formulations, the peaks of other substances were not as clear as those of SCA. The specific peaks of DDAB were at 2915, 2850, and 1465 cm^{-1}, which were also present in the SLN spectrum, indicating that DDAB was located on the SLN surface; the ZP values of formulations in Fig. 1b confirmed the presence of DDAB on SLN surface. Additionally, the peaks and patterns associated with IBU and PTX also appeared in the spectrum of the SLN formulation, although the peaks and patterns of PTX were not as clear as those of IBU. After homogenization, PTX was distributed more deeply within the lipid core than IBU because IBU is more hydrophilic than PTX. Finally, the peaks and patterns in the FT-IR spectrum of HA were predominant in those of SLN-HA, which suggested that HA covered the SLN with a relatively thick layer. Indeed, the particle sizes of SLN and SLN-HA were 72 and 169 nm, respectively. Therefore, the SLN-HA spectrum contained the dominant peaks and patterns of HA, whereas those of the other substances were simply blended into one another. This also showed the ability of HA to protect the encapsulated drugs during the delivery process to specified targets.

In vitro drug release

As a drug delivery system, SLN possesses the advantage of controlled drug release, which significantly improves the drug efficacy. The in vitro release profiles of PTX and IBU at a specific ratio from SLN and SLN-HA are shown in Fig. 2d. The drug release profiles showed an initial burst release, especially pronounced in the case of IBU, which was followed by a period of sustained release. The drug molecules positioned outside and close to the SLN surface comprised the burst release, whereas those that had been entrapped deep within the lipid core were released in a sustained manner. In the current study, after 12 h, less than 20% of PTX was released from SLN-HA, which was significantly lower than in the case of SLN. This clarified the role of HA, which was to establish a more stable shell for SLN that restricted the overall release.

In vitro cytotoxic activities

In this study, various combinations of PTX and IBU were used in order to investigate the possibility of any potential synergistic effects. The effects of in vitro exposure to the drugs separately (IBU and PTX alone) were compared with those of the PTX and IBU combinations of 1:2, 1:4, 1:6, 1:8, and 1:10 ratios (w/w) at three different concentrations, where the PTX concentrations were 1, 5, and 10 μg/mL and the IBU concentrations were prepared based on the above ratios. The CI results are presented in Fig. 3a.

All three ratios produced CI values under 1.0, which indicated that the combinations produced synergistic

effects. In addition, the CI values were lowest for the molar drug ratio of 1:4 in both cell lines. Therefore, a PTX/IBU ratio of 1:4 was selected for further experiments including assays of the cell viability, cellular uptake, and apoptosis.

The effects of SLN and SLN-HA were studied in comparison to those of the cocktail of free drugs. SLN and SLN-HA with a loaded drug ratio of 1:4 were prepared at five different concentrations in the range from 0.1 to 10 μg/mL. The cell viability after incubation with the combination of free IBU and PTX, SLN, and SLN-HA formulations for 24 and 48 h are presented in Fig. 3b. In all cases, the free drugs in combination and the nano-formulations showed clear dose-dependent and time-dependent effects. The safety of the blank SLN-HA was demonstrated in MDA-MB-231 and BT-474 cell lines. In addition, the CI values were calculated again based on the data of five concentrations, which resulted in values of 0.552 and 0.398 for BT-474 cells at 24 and 48 h, respectively, and 0.166 and 0.232 for MDA-MB-231 cells at 24 and 48 h, respectively. This confirmed the previous indication of synergistic activity for the combination of IBU and PTX in the treatment of breast cancer cell-lines. Lower cancer cell viability (< 20%) was achieved at higher drug concentrations (5 and 10 μg/mL), which indicated highly significant cytotoxic activity.

In contrast, the cytotoxic effects of IBU were only apparent at relatively higher concentrations. At concentrations in the range from 0.1 to 10 μg/mL, IBU showed no significant influence on cell viability. Consequently, the synergistic results reported in this research suggested that the treatment of IBU in combination with PTX may improve clinical efficacy and reduce the doses of both drugs.

After treatment with SLN, the cytotoxicity to MDA-MB-231 and BT-474 cells was notably higher than after the treatment with combination of free drugs, especially at concentrations of 5 and 10 μg/mL ($p < 0.05$, Fig. 3b). This could be explained by the small particle size of SLN (about 100 nm), which is more easily taken up into cells and then exerts cytotoxic effects. SLN-HA was more cytotoxic to MDA-MB-231 cells compared with SLN without HA, especially after 48 h incubation. However, the difference in cytotoxicity of SLN-HA and SLN was insignificant in the BT-474 cell line.

In summary, the current study showed that the combination of IBU and PTX exhibited synergistic effects. Furthermore, the SLN and SLN-HA showed great potential for $CD44^{+}$ cancer treatment.

In vitro cellular uptake

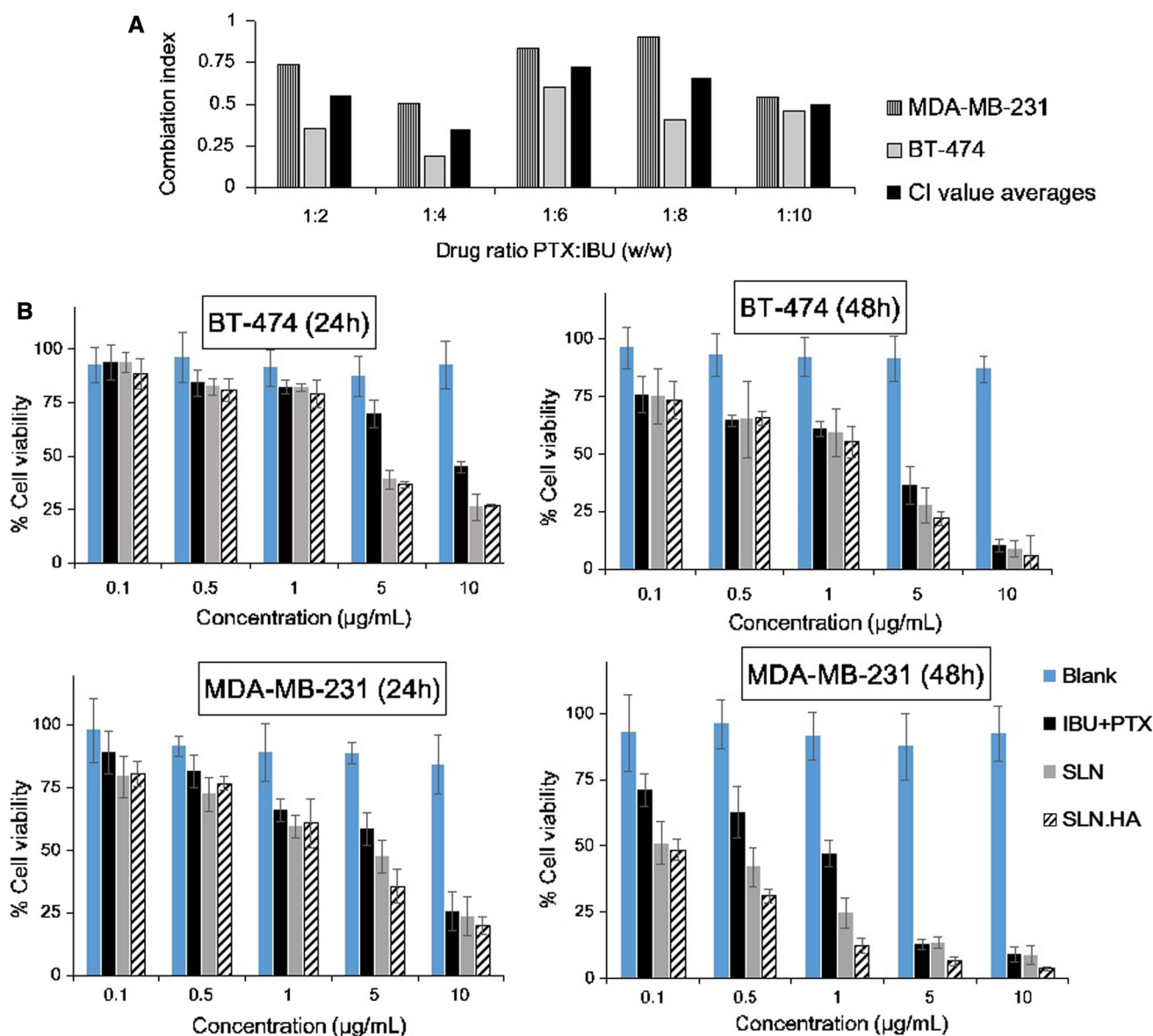To evaluate the cellular uptake of SLN and SLN-HA into cells, coumarin-6 was incorporated into nanoparticles as

Fig. 3 Cell viability assay: **a** CI values at different drug ratio (w/w) and **b** cytotoxicity assay for the selected ratio

the florescent agent. Flow cytometric analysis and confocal microscopy were performed for both BT-474 and MDA-MB-231 cell lines, which are CD44$^-$ and CD44$^+$, respectively.

The results of the flow cytometric analysis are shown in Fig. 4a. At a coumarin-6 concentration of 0.5 μg/mL, the SLN-HA nanoparticle showed significantly higher uptake into MDA-MB-231 cells than that of the SLN formulation at the same conditions. However, when MDA-MB-231 cells were pretreated with HA (20 μg/mL) for 1 h to block CD44 expression in cells, the uptake of SLN-HA was reduced significantly compared to that of non-pretreatment conditions. This suggested that the presence of HA on the surface of nanoparticles could be an advantage for targeting delivery to CD44$^+$ cancer cells. In contrast, the uptake

of SLN and SLN-HA into BT-474 cells was quite similar and the fluorescence intensity observed for both formulations was quite high. As the particle size of SLN was much smaller than SLN-HA, SLN was expected to experience a higher uptake than that of SLN-HA. However, there was no significant difference between the cellular uptake of SLN and SLN-HA (Fig. 4a).

The results from CLSM are shown in Fig. 4b, in which the internalization of SLN-HA nanoparticles in cells can be clearly observed. Both MDA-MB-231 and BT-474 cells exhibited a diffuse distribution of green in the cytoplasmic region, which suggested that SLN-HA nanoparticles were mainly distributed uniformly in the entire cell cytoplasm and not in the nucleus. However, in case of the CD44$^+$ cell line, there was a significant difference detected between the
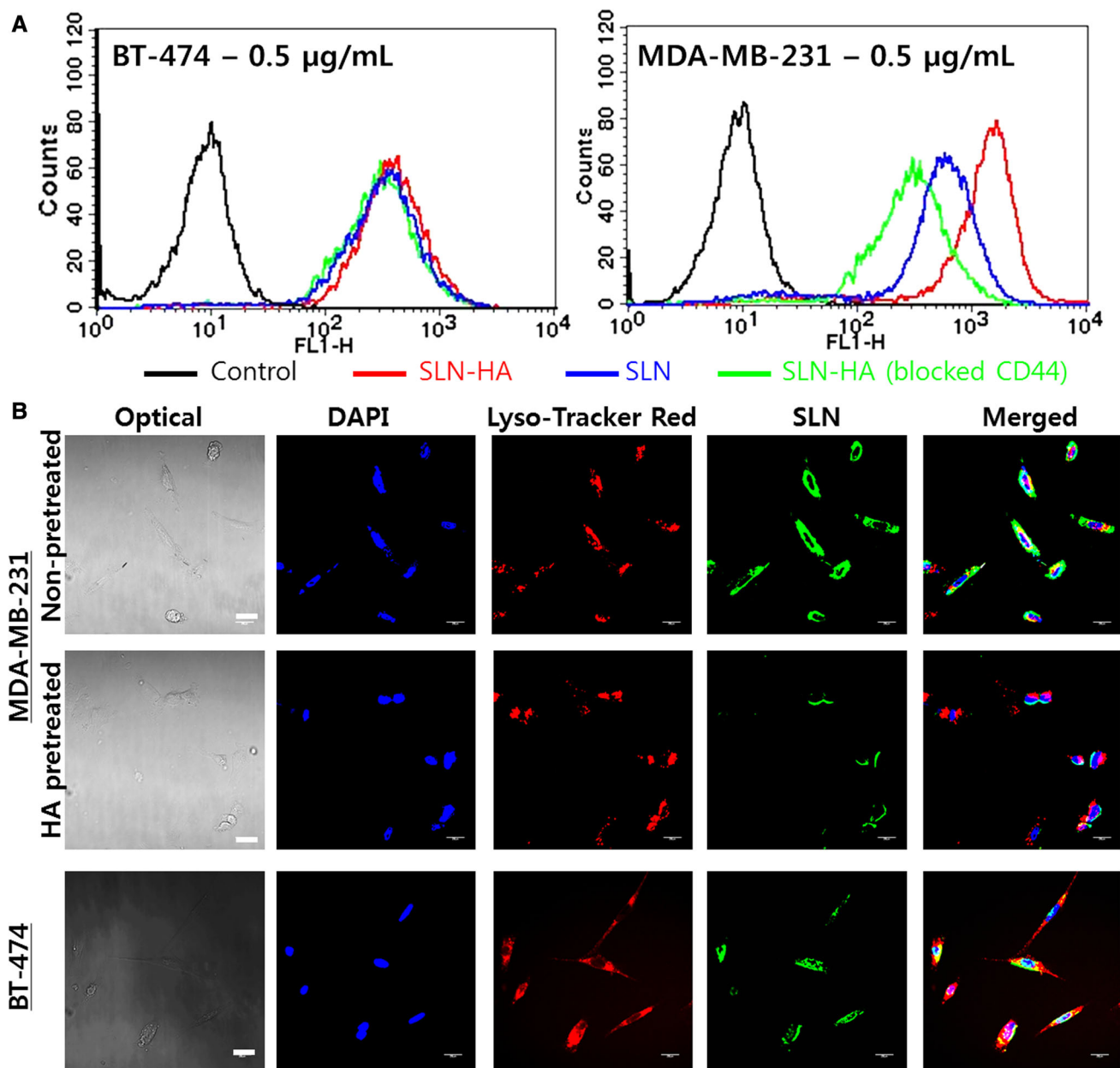
Fig. 4 a Intracellular uptake of SLN and SLN-HA labelled with coumarin-6 (0.5 μg/mL) by flow cytometry analysis and **b** confocal laser scanning microscopy (CLSM) of SLN-HA labelled with coumarin-6 (1 μg/mL). Scale bar = 20 μm

uptake of SLN-HA into cells between the HA-pretreatment and non-pretreatment conditions. The lower level of green fluorescence observed in MDA-MB-231 cells pretreated with HA was consistent with the result of flow cytometry analysis, which suggested a targeting effect of HA on the surface of SLN-HA. Furthermore, although BT-474 was a CD44⁻ cell-line, the high uptake of SLN-HA into BT-474 was suggestive of a promising application for this formulation.

In general, SLN and SLN-HA were suitable platforms for the delivery of IBU and PTX into cancer cells, in which

HA conjugation onto the nanoparticle improved the cellular uptake.

Apoptosis study

The results of the apoptosis studies are presented in Fig. 5: Fig. 5a shows results from flow cytometric study and Fig. 5b shows nuclear apoptosis determined by Hoechst staining. The cells were treated with free IBU, free PTX, the mixture of free drugs, SLN, and SLN-HA for 24 h, and then washed with PBS. The mixture of free drugs, SLN, and SLN-HA were prepared at a PTX:IBU ratio of 1:4 (w/
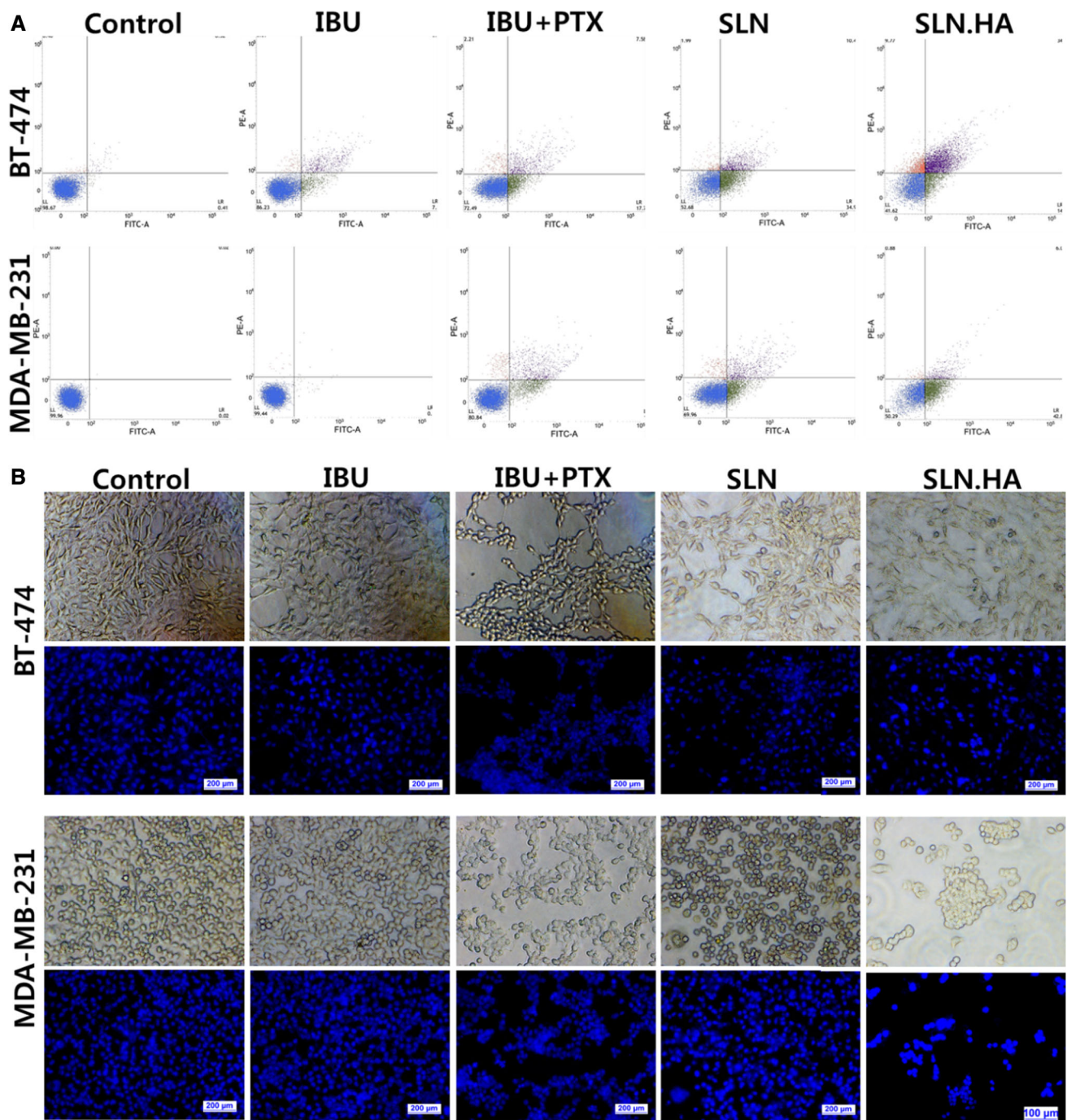
Fig. 5 Apoptosis study (concentration of 1 μg/mL): **a** flow cytometry analysis and **b** confocal laser scanning microscopy (CLSM)

w), which was selected based on the previous cell viability study (MTT assay). The flow cytometric analysis results for cells incubated with IBU and control samples were similar, which established that IBU had a low cytotoxicity at the selected concentration. These results were in good agreement with those of the cell viability assay. Conversely, both the combination of the free drugs and the nano-formulations showed remarkable apoptotic effects. The level of apoptosis inducted by treatment with the

combination of free drugs was comparatively lower than that of SLN and SLN-HA treatment; SLN-HA exerted the strongest apoptotic effect. As stated previously, CD44 plays a key role in the uptake of SLN-HA into MDA-MB-231 cells, which presumably induced a stronger early apoptotic effect in SLN-HA compared to SLN or the free drug combination. In general, the use of the nanoparticle delivery system improved the targeted uptake of these

drugs inside the cell, with a particular contribution of HA to increased SLN uptake.

In addition, the CLSM revealed the pattern of cell death based on Hoechst staining intensity, because during cell death, the cells shrink and the intracellular density rises. The nuclear condensation events that result from stress are one of the most important signatures of cytotoxicity and were observed under a fluorescence microscope after staining (Fig. 5b). Generally, the morphology of the cells after treatment with the combination of the drugs, SLN and SLN-HA, showed condensed nuclei, which supported the results obtained from the flow cytometric analysis. The difference between SLN-HA and SLN treatment was more significant in MDA-MB-231 cells than in BT-474 cells, which suggested the efficiency of CD44-targeted delivery for treatment of cancer with high CD44 expression.

Discussion

PTX- and IBU-loaded SLN were prepared by a hot-melt o/w emulsion technique, in which the lipid SCA was melted to dissolve the drugs and surfactants. As the surface of the SLN was modified with negatively-charged HA, the ZP value is deemed the most important factor for the characterization of the SLN-HA (Tran et al. 2014; Pradhan et al. 2015). T80 was used to fabricate the shearing force to make smaller lipid droplets, but the use of T80 at a relatively high concentration (3%) decreased SLN stability (Wu et al. 2011; Nguyen et al. 2015).

HA, a linear polysaccharide composed of alternating D-glucuronic acid and N-acetyl-D-glucosamine units, is a negatively-charged molecule in water (Mero and Campisi 2014). Therefore, HA can form a coating layer over the surface of the positively-charged SLN via electrostatic interaction. The successful coating of the negatively-charged HA onto the SLN surface emphasized the important role of the positively-charged surfactant (DDAB). The HA coating layer on the surface of SLN prolonged the release of drug from the nanoparticles compared with the SLN formulation, which was similar to previous reports (Tran et al. 2014, 2016; Pradhan et al. 2015).

The presence of HA on the surface of nanoparticles could be a benefit for a targeted delivery to CD44^{+} cancer cells. The fluorescence intensity was reduced when MDA-MB-231 cells were pretreated with HA, which can be explained by the different levels of CD44 expression in these cell lines. The MDA-MB-231 cell line has been reported to highly overexpress CD44, whereas a low expression level of CD44 protein was detected in BT-474 cell line (Sheridan et al. 2006; Murohashi et al. 2010; Jin et al. 2016). Therefore, there was a significant difference in uptake between cells pretreated with HA and those that were not pretreated in the MDA-MB-231 cell line. In contrast, there was no significant difference in the uptake between pretreatment with and without HA in the BT-474 cell line. The uptake of SLN-HA was higher in MDA-MB-231 cell line than in BT-474 cell line. The lower uptake level observed in BT-474 cells could be explained by passive diffusion, especially when the NPs were smaller than 200 nm (Panyam and Labhasetwar 2003; Danhier et al. 2009).

The ratio between IBU and PTX for the synergistic effect was investigated based on the CI value, which was calculated from the methods of Chou and Talalay methods (1981, 1984). The antitumor mechanisms of IBU were established in previous studies: a high concentration of IBU was required to exert cytotoxic effects (Cuzick et al. 2009; Endo et al. 2014). In this study, IBU showed no significant influence on cell viability at concentrations in the range from 0.1 to 10 μg/mL, which was consistent with results reported by other researchers (Smalley and DuBois 1997; Endo et al. 2014).

The synergic results at a PTX/IBU ratio of 1:4 suggested that treatment with the combination of IBU and PTX may improve clinical the effect and reduce the required doses of both the drugs. In addition, SLN and SLN-HA formulations showed a significant higher cytotoxicity on MDA-MB-231 and BT-474 cell lines than the mixture of free drugs.

The findings of both the MTT assay and apoptosis assay suggested the important role of HA in the enhancement of the cellular uptake and the induction of cytotoxicity via CD44 interaction (Mero and Campisi 2014; Tran et al. 2014). SLN-HA caused greater inhibition of the growth of the MDA-MB-231 cell line than SLN owing to the high expression level of CD44 in that cell. However, as the uptake of SLN and SLN-HA on BT-474 was not significantly different, the difference in apoptosis and cell inhibition was not obvious between SLN and SLN-HA formulations.

In the present study, HA was successfully coated onto the surface of SLNs by electrostatic forces. The resultant SLN-HA nanoparticles were spherical in shape and uniform in size, with a relatively thick HA shell layer. The ZP of SLN-HA was negative (− 10.5 mV) in contrast with the positive ZP of SLN, which was confirmation of the location of HA on the surface of the SLN. As predicted, drug release was more controlled and slower in SLN-HA than in SLN, possibly because of the outer HA layers. The combination of IBU and PTX showed a synergistic effect (with CI < 1.0). The improved performance of SLN-HA suggested the role of HA in targeting CD44^{+} breast cancer cell lines. Consequently, our results indicated that SLN-HA could be a potential candidate for development as a targeted drug delivery system with high bioavailability.

Compliance with ethical standards

Conflict of interest The authors declare no conflict of interest.

References

Arpicco S, Lerda C, Dalla Pozza E, Costanzo C, Tsapis N, Stella B, Donadelli M, Dando I, Fattal E, Cattel L (2013) Hyaluronic acid-coated liposomes for active targeting of gemcitabine. Eur J Pharm Biopharm 85:373–380

Basakran NS (2015) CD44 as a potential diagnostic tumor marker. Saudi Med J 36:273–279

Chou TC (2006) Theoretical basis, experimental design, and computerized simulation of synergism and antagonism in drug combination studies. Pharmacol Rev 58:621–681

Chou TC, Talalay P (1981) Generalized equations for the analysis of inhibitions of Michaelis–Menten and higher-order kinetic systems with two or more mutually exclusive and nonexclusive inhibitors. Eur J Biochem 115:207–216

Chou T-C, Talalay P (1984) Quantitative analysis of dose–effect relationships: the combined effects of multiple drugs or enzyme inhibitors. Adv Enzym Regul 22:27–55

Cuzick J, Otto F, Baron JA, Brown PH, Burn J, Greenwald P, Jankowski J, La Vecchia C, Meyskens F, Senn HJ (2009) Aspirin and non-steroidal anti-inflammatory drugs for cancer prevention: an international consensus statement. Lancet Oncol 10:501–507

Danhier F, Lecouturier N, Vroman B, Jérôme C, Marchand-Brynaert J, Feron O, Préat V (2009) Paclitaxel-loaded PEGylated PLGA-based nanoparticles: in vitro and in vivo evaluation. J Control Release 133:11–17

Endo H, Yano M, Okumura Y, Kido H (2014) Ibuprofen enhances the anticancer activity of cisplatin in lung cancer cells by inhibiting the heat shock protein 70. Cell Death Dis 5:e1027

Esposito G, Geninatti Crich S, Aime S (2008) Efficient cellular labeling by CD44 receptor-mediated uptake of cationic liposomes functionalized with hyaluronic acid and loaded with MRI contrast agents. ChemMedChem 3:1858–1862

Fonseca C, Simoes S, Gaspar R (2002) Paclitaxel-loaded PLGA nanoparticles: preparation, physicochemical characterization and in vitro anti-tumoral activity. J Control Release 83:273–286

Garud A, Singh D, Garud N (2012) Solid lipid nanoparticles (SLN): method, characterization and applications. Int Curr Pharm J 1:384–393

Götte M, Yip GW (2006) Heparanase, hyaluronan, and CD44 in cancers: a breast carcinoma perspective. Cancer Res 66:10233–10237

Harris RE, Alshafie GA, Abou-Issa H, Seibert K (2000) Chemoprevention of breast cancer in rats by celecoxib, a cyclooxygenase 2 inhibitor. Cancer Res 60:2101–2103

Hayward SL, Wilson CL, Kidambi S (2016) Hyaluronic acid-conjugated liposome nanoparticles for targeted delivery to CD44 overexpressing glioblastoma cells. Oncotarget 7:34158

Jin J, Krishnamachary B, Mironchik Y, Kobayashi H, Bhujwalla ZM (2016) Phototheranostics of CD44-positive cell populations in triple negative breast cancer. Sci Rep 6:27871

Mero A, Campisi M (2014) Hyaluronic acid bioconjugates for the delivery of bioactive molecules. Polymers 6:346–369

Mueller RH, Maeder K, Gohla S (2000) Solid lipid nanoparticles (SLN) for controlled drug delivery—a review of the state of the art. Eur J Pharm Biopharm 50:161–177

Murohashi M, Hinohara K, Kuroda M, Isagawa T, Tsuji S, Kobayashi S, Umezawa K, Tojo A, Aburatani H, Gotoh N (2010) Gene set enrichment analysis provides insight into novel signalling pathways in breast cancer stem cells. Br J Cancer 102:206–212

Naseri N, Valizadeh H, Zakeri-Milani P (2015) Solid lipid nanoparticles and nanostructured lipid carriers: structure, preparation and application. Adv Pharm Bull 5:305–313

Nguyen HT, Tran TH, Kim JO, Yong CS, Nguyen CN (2015) Enhancing the in vitro anti-cancer efficacy of artesunate by loading into poly-D, L-lactide-co-glycolide (PLGA) nanoparticles. Arch Pharm Res 38:716–724

Nguyen HT, Tran TH, Thapa RK, Pham TT, Jeong J-H, Youn YS, Choi H-G, Yong CS, Kim JO (2017) Incorporation of chemotherapeutic agent and photosensitizer in a low temperature-sensitive liposome for effective chemo-hyperthermic anti-cancer activity. Expert Opin Drug Deliv 14:155–164

Ouakrim DA, Dashti SG, Chau R, Buchanan DD, Clendenning M, Rosty C, Winship IM, Young JP, Giles GG, Leggett B (2015) Aspirin, ibuprofen, and the risk for colorectal cancer in Lynch syndrome. J Natl Cancer Inst. https://doi.org/10.1093/jnci/djv170

Panyam J, Labhasetwar V (2003) Dynamics of endocytosis and exocytosis of poly (D, L-lactide-co-glycolide) nanoparticles in vascular smooth muscle cells. Pharm Res 20:212–220

Ponta H, Sherman L, Herrlich PA (2003) CD44: from adhesion molecules to signalling regulators. Nat Rev Mol Cell Biol 4:33–45

Potta SG, Minemi S, Nukala RK, Peinado C, Lamprou DA, Urquhart A, Douroumis D (2011) Preparation and characterization of ibuprofen solid lipid nanoparticles with enhanced solubility. J Microencapsul 28:74–81

Pradhan R, Ramasamy T, Choi JY, Kim JH, Poudel BK, Tak JW, Nukolova N, Choi H-G, Yong CS, Kim JO (2015) Hyaluronic acid-decorated poly (lactic-co-glycolic acid) nanoparticles for combined delivery of docetaxel and tanespimycin. Carbohydr Polym 123:313–323

Ravar F, Saadat E, Gholami M, Dehghankelishadi P, Mahdavi M, Azami S, Dorkoosh FA (2016) Hyaluronic acid-coated liposomes for targeted delivery of paclitaxel, in vitro characterization and in vivo evaluation. J Control Release 229:10–22

Segura T, Anderson BC, Chung PH, Webber RE, Shull KR, Shea LD (2005) Crosslinked hyaluronic acid hydrogels: a strategy to functionalize and pattern. Biomaterials 26:359–371

Sheridan C, Kishimoto H, Fuchs RK, Mehrotra S, Bhat-Nakshatri P, Turner CH, Goulet R Jr, Badve S, Nakshatri H (2006) CD44+/CD24− breast cancer cells exhibit enhanced invasive properties: an early step necessary for metastasis. Breast Cancer Res 8:R59

Sherman L, Sleeman J, Herrlich P, Ponta H (1994) Hyaluronate receptors: key players in growth, differentiation, migration and tumor progression. Curr Opin Cell Biol 6:726–733

Smalley WE, DuBois RN (1997) Colorectal cancer and nonsteroidal anti-inflammatory drugs. Adv Pharmacol 39:1–20

Sutaria D, Grandhi BK, Thakkar A, Wang J, Prabhu S (2012) Chemoprevention of pancreatic cancer using solid-lipid nanoparticulate delivery of a novel aspirin, curcumin and sulforaphane drug combination regimen. Int J Oncol 41:2260–2268

Taketo MM (1998a) Cyclooxygenase-2 inhibitors in tumorigenesis (part I). J Natl Cancer Inst 90:1529–1536

Taketo MM (1998b) Cyclooxygenase-2 inhibitors in tumorigenesis (Part II). J Natl Cancer Inst 90:1609–1620

Thakkar A, Chenreddy S, Wang J, Prabhu S (2015) Evaluation of ibuprofen loaded solid lipid nanoparticles and its combination regimens for pancreatic cancer chemoprevention. Int J Oncol 46:1827–1834

Thapa RK, Choi JY, Poudel BK, Hiep TT, Pathak S, Gupta B, Choi H-G, Yong CS, Kim JO (2015) Multilayer-coated liquid crystalline nanoparticles for effective sorafenib delivery to hepatocellular carcinoma. ACS Appl Mater Interfaces 7:20360–20368

Thapa RK, Nguyen HT, Jeong J-H, Shin BS, Ku SK, Choi H-G, Yong CS, Kim JO (2017) Synergistic anticancer activity of combined histone deacetylase and proteasomal inhibitor-loaded zein nanoparticles in metastatic prostate cancers. Nanomed Nanotechnol Biol Med 13:885–896

Toole BP (2009) Hyaluronan–CD44 interactions in cancer: paradoxes and possibilities. Clin Cancer Res 15:7462–7468

Tran TH, Choi JY, Ramasamy T, Truong DH, Nguyen CN, Choi H-G, Yong CS, Kim JO (2014) Hyaluronic acid-coated solid lipid nanoparticles for targeted delivery of vorinostat to CD44 overexpressing cancer cells. Carbohydr Polym 114:407–415

Tran TH, Nguyen HT, Pham TT, Choi JY, Choi H-G, Yong CS, Kim JO (2015) Development of a graphene oxide nanocarrier for dual-drug chemo-phototherapy to overcome drug resistance in cancer. ACS Appl Mater Interfaces 7:28647–28655

Tran TH, Nguyen TD, Van Nguyen H, Nguyen HT, Kim JO, Yong CS, Nguyen CN (2016) Targeted and controlled drug delivery system loading artesunate for effective chemotherapy on CD44 overexpressing cancer cells. Arch Pharmacal Res 39:687–694

Tran TH, Nguyen HT, Phuong Tran TT, Ku SK, Jeong JH, Choi HG, Yong CS, Kim JO (2017) Combined photothermal and photodynamic therapy by hyaluronic acid-decorated polypyrrole nanoparticles. Nanomedicine (Lond) 12:1511–1523

Watanabe O, Kinoshita J, Shimizu T, Imamura H, Hirano A, Okabe T, Aiba M, Ogawa K (2005) Expression of a CD44 variant and VEGF-C and the implications for lymphatic metastasis and long-term prognosis of human breast cancer. J Exp Clin Cancer Res CR 24:75–82

Wood PL, Khan MA, Smith T, Goodenowe DB (2011) Cellular diamine levels in cancer chemoprevention: modulation by ibuprofen and membrane plasmalogens. Lipids Health Dis 10:214–222

Wu L, Zhang J, Watanabe W (2011) Physical and chemical stability of drug nanoparticles. Adv Drug Deliv Rev 63:456–469

Yao M, Zhou W, Sangha S, Albert A, Chang AJ, Liu TC, Wolfe MM (2005) Effects of nonselective cyclooxygenase inhibition with low-dose ibuprofen on tumor growth, angiogenesis, metastasis, and survival in a mouse model of colorectal cancer. Clin Cancer Res 11:1618–1628